2024 American Control Conference (ACC)
July 8-12, 2024. Toronto, Canada

Data-Driven Retrospective-Cost-Based Adaptive Digital PID Control

Yin Yong Chee, Juan A. Paredes and Dennis S. Bernstein

Abstract— **This paper develops an adaptive digital controller for sampled-data systems with unknown dynamics. The adaptive digital PID controller is based on data-driven retrospective cost adaptive control (DDRCAC) with online closed-loop system identification. Online system identification is based on recursive least squares (RLS) with variable-rate forgetting (VRF), which is used to construct a target model that provides the controller based on retrospective cost adaptive control (RCAC) with the required modeling information. For SISO plants, this modeling information includes the sign of the leading numerator coefficient as well as nonminimum-phase (NMP) zeros. The present paper illustrates the performance of DDRCAC-based digital PID control on a first-order linear plant with unknown gain sign, a NMP second-order linear plant, and a multicopter with unknown dynamics.**

I. Introduction

PID control provides a simple technique for following setpoint commands and rejecting step disturbances, and thus is the most widely used feedback control algorithm [1], [2]. Despite its simplicity, a PID controller must be tuned to ensure closed-loop stability and respect actuator magnitude constraints [3], [4]. Not surprisingly, numerous techniques have been proposed for online PID controller tuning for continuous-time [5]–[10] and discrete-time [11]–[14].

The present paper develops an adaptive PID controller as a special case of a more general adaptive control technique. In particular, we consider retrospective cost adaptive control (RCAC), which re-optimizes the coefficients of the feedback controller at each step [15]. For SISO plants, RCAC requires limited modeling information, specifically, the leading numerator coefficient and nonminimum-phase zeros. RCAC was specialized to PID control in [16], where it was applied to first-order-lag plants with deadtime as well as monotonic input and output nonlinearities. Furthermore, adaptive autopilots based on RCAC/PID controllers were implemented in multicopters [17], [18] and fixed-wing aircraft [19] for adaptive trajectory tracking.

More recently, the need for modeling information by RCAC was further mitigated by data-driven RCAC (DDRCAC), which uses online, closed-loop system identification to construct a plant model [20]. For system identification, DDRCAC uses recursive least squares (RLS) [21]. By including variable-rate forgetting (VRF), RLS/VRF can more quickly update the plant model when the plant is subjected to unexpected and unknown changes [22], [23].

The contribution of the present paper is to apply the data-driven approach of [21] to the PID controller structure assumed in [16]. By combining these techniques, the goal is to implement PID controllers for setpoint command following and constant disturbance rejection without the need for manual tuning of the controller gains when the plant changes.

The contents of the paper are as follows. Section II provides a statement of the control problem, which involves continuous-time dynamics under sampled-data feedback control. Section III provides a review of the adaptive digital PID controller based on RCAC, and Section IV introduces the DDRCAC-based PID controller, in which online system identification based on VRF-RLS provides a target model to RCAC. Section V presents numerical examples illustrates the performance of DDRCAC-based digital PID control, in particular, a first-order linear plant with unknown gain sign, a NMP second-order linear plant, and a multicopter with unknown dynamics. Finally, Section VI presents conclusions.

Notation: $\mathbf{q} \in \mathbb{C}$ denotes the forward-shift operator. For all $x \in \mathbb{R}^n$, $\mathrm{diag}(x)$ yields a $n \times n$ diagonal matrix with the elements of x on the main diagonal. I_n is the $n \times n$ identity matrix, $0_{n\times m}$ is the $n \times m$ zeros matrix, and $\mathbb{1}_{n\times m}$ is the $n \times m$ ones matrix. For all $r \in \mathbb{R}$, $\mathrm{e}r \triangleq 10^r$.

II. Problem Statement

To reflect the practical implementation of digital controllers for physical systems, we consider continuous-time dynamics under sampled-data control using discrete-time adaptive (time-variant) controllers. In particular, we consider the control architecture shown in Figure 1, where $\mathcal{M}$ is the target SISO continuous-time system, $t \geq 0$, $r(t) \in \mathbb{R}$ is the command, $u(t) \in \mathbb{R}$ is the control, $d(t) \in \mathbb{R}$ is the disturbance, $v(t) \triangleq u(t) + d(t)$ is the input of $\mathcal{M}$, and $y(t) \in \mathbb{R}$ is the output of $\mathcal{M}$. In particular, r and y are sampled to produce the sampled command $r_k \in \mathbb{R}$, and the measurement $y_k \in \mathbb{R}$, respectively, which, for all $k \geq 0$, are

$$r_k \triangleq r(kT_{\mathrm{s}}), \tag{1}$$

$$y_k \triangleq y(kT_{\mathrm{s}}), \tag{2}$$

where $T_{\mathrm{s}} > 0$ is the sample time. The error $e_k \triangleq r_k - y_k$ is passed through the error-normalization function $\mathcal{N}\colon \mathbb{R} \to \mathbb{R}$ given by

$$\mathcal{N}(e) \triangleq \frac{e}{\nu + |e|}, \tag{3}$$

where $\nu \geq 0$, to yield the normalized error, which is used as the performance variable z_k, such that

$$z_k \triangleq \mathcal{N}(e_k). \tag{4}$$

The adaptive digital PID controller, which is updated at each step k, is denoted by $G_{\mathrm{c},k}$. The inputs to $G_{\mathrm{c},k}$ are y_k and z_k, and its output at each step k is the discrete-time control

Yin Yong Chee, Juan A. Paredes and Dennis S. Bernstein are with the Department of Aerospace Engineering, University of Michigan, Ann Arbor, MI, USA. {cyinyong, jparedes, dsbaero}@umich.edu

$u_k \in \mathbb{R}^m$. The continuous-time control signal $u(t)$ applied to the structure is generated by applying a zero-order-hold operation to u_k, that is, for all $k \geq 0$, and, for all $t \in [kT_\mathrm{s}, (k+1)T_\mathrm{s})$,

$$u(t) = u_k. \tag{5}$$

The objective of the adaptive controller is to yield an input signal that minimizes the difference between the command and the output of the continuous-time system, that is, for all $t \geq 0$, yield $u(t)$ such that $|r(t) - y(t)|$ is minimized. Note that, error-normalization is implemented to improve robustness and command tracking, as shown in [16], and, in the case where $\mathcal{M}$ is a MIMO continuous-time system, multiple PID blocks can be used, as shown in Example 5.3.

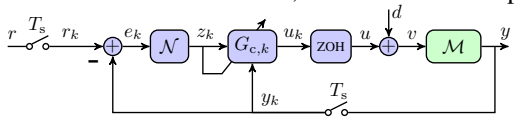

Fig. 1: Sampled-data implementation of adaptive PID controller for control of the SISO continuous-time system $\mathcal{M}$. All sample-and-hold operations are synchronous. The error $e_k \triangleq r_k - y_k$ is passed through the error-normalization function $\mathcal{N}$ shown in (3) to generate the normalized error, which is used as the performance variable z_k of the adaptive controller. The adaptive controller $G_{\mathrm{c},k}$ generates the discrete-time control u_k at each step k. The resulting continuous-time control $u(t)$ is generated by applying a zero-order-hold operation to u_k.

III. Review of Adaptive Digital PID controller

This section reviews RCAC/PID. The discrete-time requested control u_k, which is determined by the adaptive digital PID controller, has the form

$$u_k = \kappa_{\mathrm{p},k} z_{k-1} + \kappa_{\mathrm{i},k} \zeta_{k-1} + \kappa_{\mathrm{d},k}(z_{k-1} - z_{k-2}), \tag{6}$$

where $\kappa_{\mathrm{p},k}$, $\kappa_{\mathrm{i},k}$, and $\kappa_{\mathrm{d},k}$ are time-varying PID gains and ζ_k is given by the anti-windup integrator

$$\zeta_k \triangleq \sum_{j=0}^{k} z_j - \begin{cases} \left(\operatorname{sign} \sum_{j=0}^{k} z_j\right)(\underline{u} - u_k), & u_k < \underline{u}, \\ 0, & \underline{u} \leq u_k \leq \overline{u}, \\ \left(\operatorname{sign} \sum_{j=0}^{k} z_j\right)(u_k - \overline{u}), & u_k > \overline{u}, \end{cases} \tag{7}$$

where $\underline{u} < \overline{u}$ are the respective lower and upper anti-windup thresholds. In this paper, $\overline{u} = -\underline{u} = 50$ since the effects of saturation are not considered in this work. A related anti-windup technique is given in [24, p. 310–311]. The control (6) can be expressed as

$$u_k = \phi_{\mathrm{c},k} \theta_{\mathrm{c},k}, \tag{8}$$

where

$$\phi_{\mathrm{c},k} \triangleq \begin{bmatrix} z_{k-1} & \zeta_{k-1} & z_{k-1} - z_{k-2} \end{bmatrix} \in \mathbb{R}^{1\times 3}, \tag{9}$$

$$\theta_{\mathrm{c},k} \triangleq \begin{bmatrix} \kappa_{\mathrm{p},k} & \kappa_{\mathrm{i},k} & \kappa_{\mathrm{d},k} \end{bmatrix}^{\mathsf{T}} \in \mathbb{R}^3. \tag{10}$$

Note that the regressor $\phi_{\mathrm{c},k}$ is constructed from the past values of z_k and ζ_k, and the controller coefficient vector $\theta_{\mathrm{c},k}$ contains the time-dependent proportional, integral, and derivative gains $\kappa_{\mathrm{p},k}$, $\kappa_{\mathrm{i},k}$, and $\kappa_{\mathrm{d},k}$. Furthermore, note that the adaptive digital PID control can be specialized to adaptive digital PI, PD, ID, P, I, and D control by omitting the corresponding components of $\phi_{\mathrm{c},k}$ and $\theta_{\mathrm{c},k}$.

Next, define the retrospective cost variable

$$\tilde{z}_k(\tilde{\theta}) \triangleq z_k - G_\mathrm{f}(\mathbf{q})(u_k - \phi_{\mathrm{c},k}\tilde{\theta}_\mathrm{c}), \tag{11}$$

where G_f is a SISO asymptotically stable, strictly proper transfer function, and $\tilde{\theta}_\mathrm{c} \in \mathbb{R}^3$ is the controller coefficient vector determined by optimization below. The rationale underlying (11) is to replace the applied past control inputs with the re-optimized control input $\phi_{\mathrm{c},k}\tilde{\theta}_\mathrm{c}$ so that the closed-loop transfer function from $u_k - \phi_{\mathrm{c},k}\theta_{\mathrm{c},k+1}$ to z_k matches G_f [15], [20]. Consequently, G_f serves as a closed-loop target model for adaptation.

In the present paper, G_f is chosen to be a finite-impulse-response transfer function of window length n_f of the form

$$G_\mathrm{f}(\mathbf{q}) \triangleq \sum_{i=1}^{n_\mathrm{f}} N_i \mathbf{q}^{-i}, \tag{12}$$

where $N_1, \ldots, N_{n_\mathrm{f}} \in \mathbb{R}$. We can thus rewrite (11) as

$$\tilde{z}_k(\tilde{\theta}) = z_k - N(\bar{U}_k - \bar{\phi}_{\mathrm{c},k}\tilde{\theta}_\mathrm{c}), \tag{13}$$

where

$$\bar{\phi}_{\mathrm{c},k} \triangleq \begin{bmatrix} \phi_{\mathrm{c},k-1} \\ \vdots \\ \phi_{\mathrm{c},k-n_\mathrm{f}} \end{bmatrix} \in \mathbb{R}^{n_\mathrm{f}\times 3}, \; \bar{U}_k \triangleq \begin{bmatrix} u_{k-1} \\ \vdots \\ u_{k-n_\mathrm{f}} \end{bmatrix} \in \mathbb{R}^{n_\mathrm{f}}, \tag{14}$$

$$N \triangleq \begin{bmatrix} N_1 & \cdots & N_{n_\mathrm{f}} \end{bmatrix} \in \mathbb{R}^{1\times n_\mathrm{f}}. \tag{15}$$

The choice of N includes all required modeling information. Since the plant is SISO in this work, this information consists of the sign of the leading numerator coefficient, the relative degree of the sampled-data system, and all nonminimum-phase (NMP) zeros [15], [20]. Since zeros are invariant under feedback, omission of a NMP zero from G_f may entail unstable pole-zero cancellation. Cancellation can be prevented, however, by using the control weighting R_u introduced below, as discussed in [15], [25]. In [16], $N = \sigma$, where $\sigma \in \{-1, 1\}$. Note that N can be constructed and updated online using data, as shown in Section IV.

Using (11), we define the retrospective cost function

$$J_{\mathrm{c},k}(\tilde{\theta}_\mathrm{c}) \triangleq \sum_{i=0}^{k} [\tilde{z}_i^2(\tilde{\theta}_\mathrm{c}) + R_u(\phi_{\mathrm{c},k}\tilde{\theta}_\mathrm{c})^2] + (\tilde{\theta}_\mathrm{c} - \theta_{\mathrm{c},0})^{\mathrm{T}} P_{\mathrm{c},0}^{-1}(\tilde{\theta}_\mathrm{c} - \theta_{\mathrm{c},0}), \tag{16}$$

where $\theta_{\mathrm{c},0} \in \mathbb{R}^3$ is the initial vector of PID gains, $P_{\mathrm{c},0} \in \mathbb{R}^{3\times 3}$ is positive definite, and $R_u \geq 0$. As can be seen from (8), R_u serves as a control weighting, which prevents RCAC from cancelling unmodeled NMP zeros, and the matrix $P_{\mathrm{c},0}^{-1}$ defines the regularization term and initializes the recursion for $P_{\mathrm{c},k}$ defined below.

Next, it follows from recursive least squares (RLS) minimization [21] that, for all $k \geq 0$, the unique global minimizer $\theta_{\mathrm{c},k+1}$ of (16) is given by

$$P_{\mathrm{c},k+1} = P_{\mathrm{c},k} - P_{\mathrm{c},k} \begin{bmatrix} N\bar{\phi}_{\mathrm{c},k} \\ \phi_{\mathrm{c},k} \end{bmatrix}^{\mathsf{T}} \Gamma_{\mathrm{c},k} \begin{bmatrix} N\bar{\phi}_{\mathrm{c},k} \\ \phi_{\mathrm{c},k} \end{bmatrix} P_{\mathrm{c},k}, \tag{17}$$

$$\theta_{\mathrm{c},k+1} = \theta_{\mathrm{c},k} - P_{\mathrm{c},k+1} \begin{bmatrix} N\bar{\phi}_{\mathrm{c},k} \\ \phi_{\mathrm{c},k} \end{bmatrix}^{\mathsf{T}} \bar{R} \begin{bmatrix} z_k - N(\bar{U}_k - \bar{\phi}_{\mathrm{c},k}\theta_{\mathrm{c},k}) \\ \phi_{\mathrm{c},k}\theta_{\mathrm{c},k} \end{bmatrix}, \tag{18}$$

where

$$\Gamma_{\mathrm{c},k} \triangleq \bar{R} - \bar{R}\begin{bmatrix} N\bar{\phi}_{\mathrm{c},k} \\ \phi_{\mathrm{c},k} \end{bmatrix} \Xi_{\mathrm{c},k}^{-1} \begin{bmatrix} N\bar{\phi}_{\mathrm{c},k} \\ \phi_{\mathrm{c},k} \end{bmatrix}^{\mathsf{T}} \bar{R} \in \mathbb{R}^{2\times 2}, \tag{19}$$

$$\Xi_{\mathrm{c},k} \triangleq P_{\mathrm{c},k}^{-1} + \begin{bmatrix} N\bar{\phi}_{\mathrm{c},k} \\ \phi_{\mathrm{c},k} \end{bmatrix}^{\mathsf{T}} \bar{R} \begin{bmatrix} N\bar{\phi}_{\mathrm{c},k} \\ \phi_{\mathrm{c},k} \end{bmatrix} \in \mathbb{R}^{2\times 2}, \tag{20}$$

$$\bar{R} \triangleq \operatorname{diag}(1, R_u) \in \mathbb{R}^{2\times 2}. \tag{21}$$

To update (17) and (18), let the initial conditions be $z_{-3} = z_{-2} = z_{-1} \triangleq 0$, $\zeta_{-1} \triangleq 0$, and $u_{-1} \triangleq 0$. The RCAC-based adaptive digital PID controller is thus given by (7), (8), (9), (10), (17), and (18). Note that this choice of initial conditions implies that $\phi_{\mathrm{c},-1} = 0$. It thus follows that $P_{\mathrm{c},1} = P_{\mathrm{c},0}$ and $\theta_{\mathrm{c},1} = \theta_{\mathrm{c},0}$. Consequently, if $\theta_{\mathrm{c},0} = 0_{3\times 1}$, then the first possibly nonzero control input is u_2. For all of the numerical simulations in this paper, $\theta_{\mathrm{c},k}$ is initialized as $\theta_{\mathrm{c},0} = 0_{3\times 1}$ to reflect the absence of additional prior modeling information. For convenience, we set $P_{\mathrm{c},0} = p_{\mathrm{c},0} I_3$, where the scalar $p_{\mathrm{c},0} > 0$ determines the initial rate of adaptation.

IV. Data-Driven Adaptive Digital PID Controller

This section introduces DDRCAC/PID, in which system identification is used to update N in (17) and (18) at each time step k. First, the RLS/VRF system identification technique is introduced.

Let $\hat{n} \geq 0$ and, for all $k \geq 0$, let $F_{\mathrm{m},1,k}, \ldots, F_{\mathrm{m},\hat{n},k} \in \mathbb{R}$ and $G_{\mathrm{m},1,k}, \ldots, G_{\mathrm{m},\hat{n},k} \in \mathbb{R}$ be the coefficient matrices to be estimated using RLS. Furthermore, let $\hat{y}_k \in \mathbb{R}^p$ be an estimate of y_k defined by

$$\hat{y}_k \triangleq -\sum_{i=1}^{\hat{n}} F_{\mathrm{m},i,k} y_{k-i} + \sum_{i=1}^{\hat{n}} G_{\mathrm{m},i,k} u_{k-i}, \tag{22}$$

where

$$y_{-\hat{n}} = \cdots = y_{-1} = 0, \tag{23}$$

$$u_{-\hat{n}} = \cdots = u_{-1} = 0. \tag{24}$$

It follows from (22) that, for all $k \geq 0$,

$$\hat{y}_k = \phi_{\mathrm{m},k} \theta_{\mathrm{m},k}, \tag{25}$$

where

$$\theta_{\mathrm{m},k} \triangleq \begin{bmatrix} F_{\mathrm{m},1,k} & \cdots & F_{\mathrm{m},\hat{n},k} & G_{\mathrm{m},1,k} & \cdots & G_{\mathrm{m},\hat{n},k} \end{bmatrix}^{\mathsf{T}} \in \mathbb{R}^{2\hat{n}}, \tag{26}$$

$$\phi_{\mathrm{m},k} \triangleq \begin{bmatrix} -y_{k-1} & \cdots & -y_{k-\hat{n}} & u_{k-1} & \cdots & u_{k-\hat{n}} \end{bmatrix} \in \mathbb{R}^{1\times 2\hat{n}}. \tag{27}$$

To determine the update equations for $\theta_{\mathrm{m},k}$, for all $k \geq 0$, define $e_{\mathrm{m},k} \colon \mathbb{R}^{2\hat{n}} \to \mathbb{R}$ by

$$e_{\mathrm{m},k}(\tilde{\theta}_{\mathrm{m}}) \triangleq y_k - \phi_{\mathrm{m},k} \tilde{\theta}_{\mathrm{m}}, \tag{28}$$

where $\tilde{\theta}_{\mathrm{m}} \in \mathbb{R}^{2\hat{n}}$. Using (25), the identification error at step k is defined by

$$e_{\mathrm{m},k}(\theta_{\mathrm{m},k}) = y_k - \hat{y}_k. \tag{29}$$

For all $k \geq 0$, the RLS identification cumulative cost is defined by

$$J_{\mathrm{m},k}(\tilde{\theta}_{\mathrm{m}}) \triangleq \sum_{i=0}^{k} \frac{\rho_i}{\rho_k} e_{\mathrm{m},i}^2(\tilde{\theta}_{\mathrm{m}}) + \frac{1}{\rho_k} (\tilde{\theta}_{\mathrm{m}} - \theta_{\mathrm{m},0})^{\mathsf{T}} P_{\mathrm{m},0}^{-1} (\tilde{\theta}_{\mathrm{m}} - \theta_{\mathrm{m},0}), \tag{30}$$

where $P_{\mathrm{m},0} \in \mathbb{R}^{2\hat{n}\times 2\hat{n}}$ is positive definite, $\theta_{\mathrm{m},0} \in \mathbb{R}^{2\hat{n}}$ is the initial estimate of the coefficient vector, and, for all $i \geq 0$,

$$\rho_i \triangleq \prod_{j=0}^{i} \lambda_j^{-1}. \tag{31}$$

For all $j \geq 0$, the parameter $\lambda_j \in (0, 1]$ is the forgetting factor defined by $\lambda_j \triangleq \beta_j^{-1}$, where

$$\beta_j \triangleq \begin{cases} 1, & j < \tau_{\mathrm{d}}, \\ 1 + \eta \bar{\beta}_j, & j \geq \tau_{\mathrm{d}}, \end{cases} \tag{32}$$

$$\bar{\beta}_j \triangleq \gamma_{\tau_{\mathrm{d}},\tau_{\mathrm{n}},j} \mathbf{1}\big(\gamma_{\tau_{\mathrm{d}},\tau_{\mathrm{n}},j}\big), \tag{33}$$

$\tau_{\mathrm{d}} > \tau_{\mathrm{n}} >= 1$, $\eta > 0$, $\mathbf{1} \colon \mathbb{R} \to \{0, 1\}$ is the unit step function, such that

$$\mathbf{1}(a) \triangleq \begin{cases} 1, & a \geq 0, \\ 0, & \text{otherwise}, \end{cases} \tag{34}$$

and

$$\gamma_{\tau_{\mathrm{d}},\tau_{\mathrm{n}},k} \triangleq \frac{\sqrt{\frac{1}{\tau_{\mathrm{n}}} \sum_{i=k-\tau_{\mathrm{n}}}^{k} e_{\mathrm{m},i}^2(\theta_{\mathrm{m},i})}}{\sqrt{\frac{1}{\tau_{\mathrm{d}}} \sum_{i=k-\tau_{\mathrm{d}}}^{k} e_{\mathrm{m},i}^2(\theta_{\mathrm{m},i})}} - 1. \tag{35}$$

Then, it follows from recursive least squares (RLS) minimization [21] that, for all $k \geq 0$, the unique global minimizer $\theta_{\mathrm{m},k+1}$ of (30) is given by

$$P_{\mathrm{m},k+1} = \beta_k P_{\mathrm{m},k} \left(I_{2\hat{n}} - \frac{\phi_{\mathrm{m},k}^{\mathsf{T}} \phi_{\mathrm{m},k}}{\frac{1}{\beta_k} + \phi_{\mathrm{m},k} P_{\mathrm{m},k} \phi_{\mathrm{m},k}^{\mathsf{T}}} P_{\mathrm{m},k} \right), \tag{36}$$

$$\theta_{\mathrm{m},k+1} = \theta_{\mathrm{m},k} + P_{\mathrm{m},k+1} \phi_{\mathrm{m},k}^{\mathsf{T}} (y_k - \phi_{\mathrm{m},k} \theta_{\mathrm{m},k}), \tag{37}$$

where $P_{\mathrm{m},0}$ is the performance-regularization weighting in (30). Additional details concerning the VRF/RLS techniques used in this work are given in [22].

Next, let $\hat{n} = n_{\mathrm{f}}$ and, for all $k \geq 0$, define $N_k \in \mathbb{R}^{1\times n_{\mathrm{f}}}$ such that

$$N_k \triangleq \begin{cases} [-1 \;\; 0_{1\times n_{\mathrm{f}}-1}], & G_{\mathrm{m},1,k} = \cdots = G_{\mathrm{m},n_{\mathrm{f}},k} = 0, \\ [G_{\mathrm{m},1,k} \;\; \cdots \;\; G_{\mathrm{m},n_{\mathrm{f}},k}], & \text{otherwise}. \end{cases} \tag{38}$$

Then, for all $k \geq 0$, replacing N with N_k in (17), and (18) yields the DDRCAC update equations

$$P_{\mathrm{c},k+1} = P_{\mathrm{c},k} - P_{\mathrm{c},k} \begin{bmatrix} N_k\bar{\phi}_{\mathrm{c},k} \\ \phi_{\mathrm{c},k} \end{bmatrix}^{\mathsf{T}} \Gamma_{\mathrm{c},k} \begin{bmatrix} N_k\bar{\phi}_{\mathrm{c},k} \\ \phi_{\mathrm{c},k} \end{bmatrix} P_{\mathrm{c},k}, \tag{39}$$

$$\theta_{\mathrm{c},k+1} = \theta_{\mathrm{c},k} - P_{\mathrm{c},k+1} \begin{bmatrix} N_k\bar{\phi}_{\mathrm{c},k} \\ \phi_{\mathrm{c},k} \end{bmatrix}^{\mathsf{T}} \bar{R} \begin{bmatrix} z_k - N_k(\bar{U}_k - \bar{\phi}_{\mathrm{c},k}\theta_{\mathrm{c},k}) \\ \phi_{\mathrm{c},k}\theta_{\mathrm{c},k} \end{bmatrix}, \tag{40}$$

where

$$\Gamma_{\mathrm{c},k} = \bar{R} - \bar{R}\begin{bmatrix} N_k\bar{\phi}_{\mathrm{c},k} \\ \phi_{\mathrm{c},k} \end{bmatrix} \Xi_{\mathrm{c},k}^{-1} \begin{bmatrix} N_k\bar{\phi}_{\mathrm{c},k} \\ \phi_{\mathrm{c},k} \end{bmatrix}^{\mathsf{T}} \bar{R} \in \mathbb{R}^{2\times 2}, \tag{41}$$

$$\Xi_{\mathrm{c},k} = P_{\mathrm{c},k}^{-1} + \begin{bmatrix} N_k\bar{\phi}_{\mathrm{c},k} \\ \phi_{\mathrm{c},k} \end{bmatrix}^{\mathsf{T}} \bar{R} \begin{bmatrix} N_k\bar{\phi}_{\mathrm{c},k} \\ \phi_{\mathrm{c},k} \end{bmatrix} \in \mathbb{R}^{2\times 2}. \tag{42}$$

The DDRCAC-based adaptive digital PID controller is thus given by (7), (8), (9), (10), (26), (27), (32), (36), (37), (38), (39), and (40). At each step k, N_k provides the numerator coefficients of the identified system to RCAC, and thus provides required modeling information such as the sign of the leading numerator coefficient as well as NMP zeros. The initial conditions for the RCAC states in DDRCAC

are the same as the ones stated in Section III. For all of the numerical simulations in this paper, $\theta_{\mathrm{m},k}$ is initialized as $\theta_{\mathrm{m},0} = 0_{3\times 1}$ to reflect the absence of additional prior modeling information. For convenience, we set $P_{\mathrm{m},0} = p_{\mathrm{m},0} I_3$, where the scalar $p_{\mathrm{m},0} > 0$ determines the initial rate of identification.

V. Numerical Examples

In this section, DDRCAC/PID is implemented in numerical simulations to illustrate its performance and compared with RCAC/PID. Example 5.1 features a first-order linear plant with unknown gain sign. Example 5.2 features a second-order linear NMP plant. Example 5.3 features a multicopter with unknown dynamics . In Examples 5.1 and 5.2, $T_{\mathrm{s}} = 0.1$ s. In Example 5.3, $T_{\mathrm{s}} = 0.001$ s. Tables I and II show the RCAC and DDRCAC hyperparameters used in the numerical examples. The same RCAC hyperparameters are used by both RCAC/PID and DDRCAC/PID controllers. In Example 5.3, a total of 6 controllers are implemented, 3 per position and velocity loop for each of the x, y, and z axes. Details are provided in Example 5.3.

TABLE I: RCAC and DDRCAC hyperparameters in Examples 5.1 and 5.2

Example	Control	$p_{\mathrm{c},0}$	R_{u}	$G_{\mathrm{f}}(\mathbf{q})$	ν	η	τ_{n}	τ_{d}	$\hat{n}$	$p_{\mathrm{m},0}$
5.1	PID	0.5	0	$\{-1/\mathbf{q}, 1/\mathbf{q}\}$	50	0.1	40	200	3	5e-4
5.2		1		$\{-1/\mathbf{q}, -(\mathbf{q}-2)/\mathbf{q}^2, -(\mathbf{q}-10)/\mathbf{q}^2\}$					2	5e-3

TABLE II: RCAC and DDRCAC hyperparameters in Example 5.3

Loop	Control	Axes	$p_{\mathrm{c},0}$	R_{u}	$G_{\mathrm{f}}(\mathbf{q})$	ν	η	τ_{n}	τ_{d}	$\hat{n}$	$p_{\mathrm{m},0}$
Position	P	x, y	0.1	0.01	$-(5\mathrm{e}{-3})/\mathbf{q}$	1	0.1	15	20	1	1
		z									
Velocity	PI	x, y	1		$\{-0.5/\mathbf{q}, 0.5/\mathbf{q}\}$						
		z			$-0.5/\mathbf{q}$						

Example 5.1: First-order linear plant with unknown gain sign. Let $\mathcal{M}$ be the first-order-lag-plus-dead-time dynamics

$$G(s) = \frac{Ke^{-\tau_{\mathrm{dt}}}}{\tau_{\mathrm{c}} s + 1}, \tag{43}$$

where $K \in \mathbb{R}$ is the DC gain, $\tau_{\mathrm{dt}} > 0$ is the dead time, and $\tau_{\mathrm{c}} > 0$ is the time constant. In this example, let $y(0) = 0$, $K = 1$, $\tau_{\mathrm{dt}} = 1$ s, and $\tau_{\mathrm{c}} \in \{0.2, 1, 5\}$ s. Then, the control objective is to follow the command

$$r(t) = \begin{cases} 8, & t \in [0, 80] \text{ s}, \\ -9, & t \in (80, 240] \text{ s}, \\ 4, & t > 240 \text{ s}, \end{cases} \tag{44}$$

in the presence of the disturbance

$$d(t) = \begin{cases} 8, & t \in [0, 160] \text{ s}, \\ 4, & t > 160 \text{ s}. \end{cases} \tag{45}$$

The results of the numerical simulations, where the control is given by RCAC/PID with $G_{\mathrm{f}}(\mathbf{q}) = -1/\mathbf{q}$, RCAC/PID with $G_{\mathrm{f}}(\mathbf{q}) = 1/\mathbf{q}$, and DDRCAC/PID, are shown in Figures 2, 3, and 4. Note that the closed-loop system is unstable when RCAC/PID is implemented with $G_{\mathrm{f}}(\mathbf{q}) = 1/\mathbf{q}$, since an incorrect gain is specified in the target model. In contrast, DDRCAC/PID does not require this information. ◇

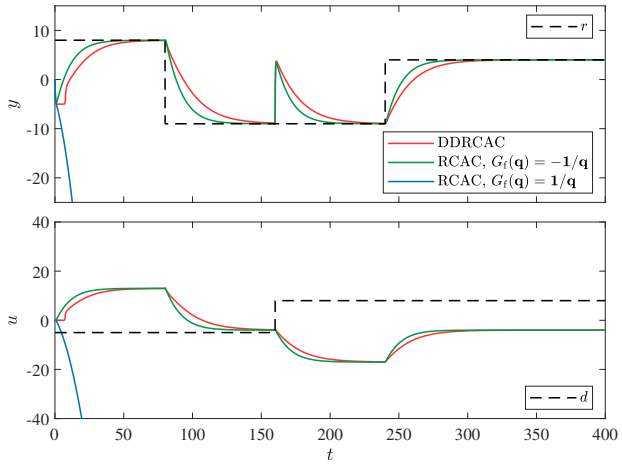

Fig. 2: Example 5.1: Control of the first-order-lag-plus-dead-time dynamics (43) with $y(0) = 0$, $K = 1$, $\tau_{\mathrm{dt}} = 1$ s, and $\tau_{\mathrm{c}} = 0.2$ s. The control is given by RCAC/PID with $G_{\mathrm{f}}(\mathbf{q}) = -1/\mathbf{q}$, RCAC/PID with $G_{\mathrm{f}}(\mathbf{q}) = 1/\mathbf{q}$, and DDRCAC/PID.

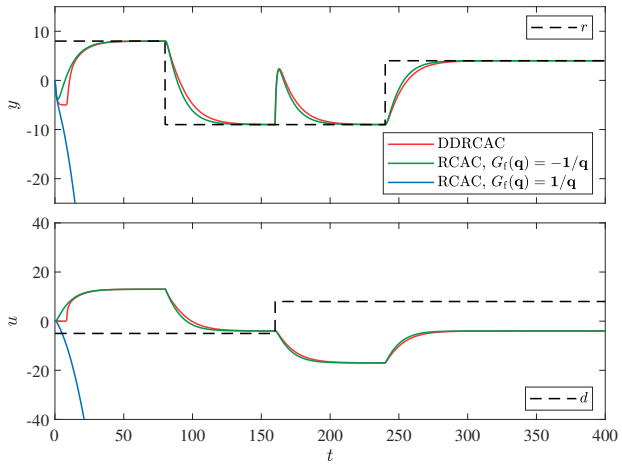

Fig. 3: Example 5.1: Control of the first-order-lag-plus-dead-time dynamics (43) with $y(0) = 0$, $K = 1$, $\tau_{\mathrm{dt}} = 1$ s and $\tau_{\mathrm{c}} = 1$ s. The control is given by RCAC/PID with $G_{\mathrm{f}}(\mathbf{q}) = -1/\mathbf{q}$, RCAC/PID with $G_{\mathrm{f}}(\mathbf{q}) = 1/\mathbf{q}$, and DDRCAC/PID.

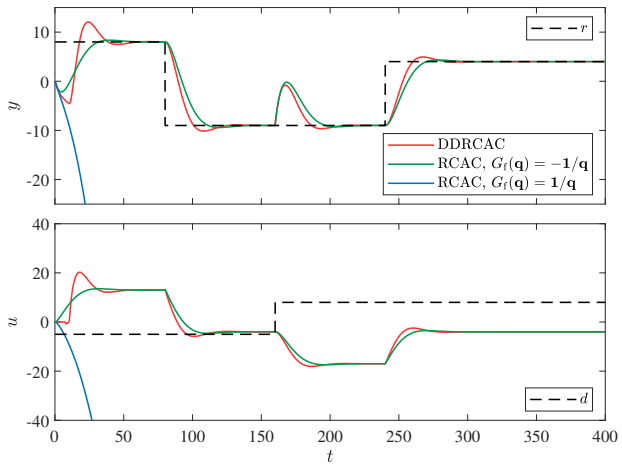

Fig. 4: Example 5.1: Control of the first-order-lag-plus-dead-time dynamics (43) with $y(0) = 0$, $K = 1$, $\tau_{\mathrm{dt}} = 1$ s, and $\tau_{\mathrm{c}} = 5$ s. The control is given by RCAC/PID with $G_{\mathrm{f}}(\mathbf{q}) = -1/\mathbf{q}$, RCAC/PID with $G_{\mathrm{f}}(\mathbf{q}) = 1/\mathbf{q}$, and DDRCAC/PID.

Example 5.2: Second-order linear NMP plant. Let $\mathcal{M}$ be the second-order linear NMP dynamics

$$G(s) = K\frac{s-b}{s^2+2\xi s+1}, \tag{46}$$

where $K \in \mathbb{R}$ is the DC gain, $b > 0$ is the NMP zero, and ξ is a damping coefficient. In this example, let $y(0) = 0$, $\dot{y}(0) = 0$, $K = 0.5$, $b = 2$ s, and $\xi \in \{0.2, 1\}$ s. Then, the control objective is to follow the command (44) in the presence of the disturbance (45)

The results of the numerical simulations, where the control is given by RCAC/PID with $G_{\mathrm{f}}(\mathbf{q}) = -1/\mathbf{q}$, RCAC/PID with $G_{\mathrm{f}}(\mathbf{q}) = -(\mathbf{q}-2)/\mathbf{q}^2$, RCAC/PID with $G_{\mathrm{f}}(\mathbf{q}) = -(\mathbf{q}-10)/\mathbf{q}^2$, and DDRCAC/PID, are shown in Figures 5 and 6. Note that the closed-loop response is unstable when RCAC/PID is implemented with $G_{\mathrm{f}}(\mathbf{q}) = -1/\mathbf{q}$ since the NMP zero is not included in the target model. This can be mitigated by including a NMP zero in G_{f} to the right of the true NMP zero, as shown in the cases in which RCAC/PID is implemented with $G_{\mathrm{f}}(\mathbf{q}) = -(\mathbf{q}-10)/\mathbf{q}^2$. In contrast, DDRCAC/PID does not require this information. ◇

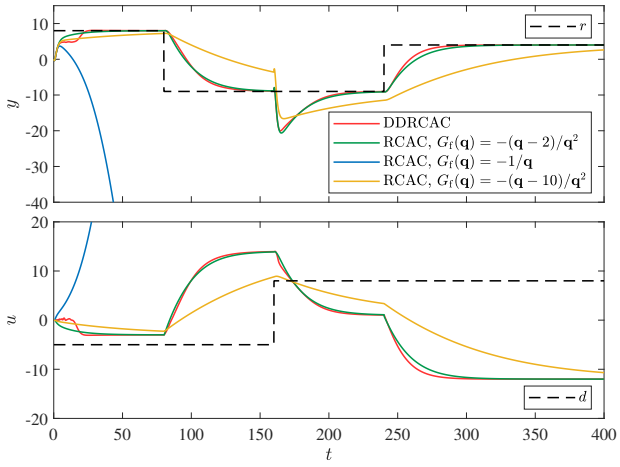

Fig. 5: Example 5.2: Control of the second-order linear NMP plant dynamics (46) with $y(0) = 0$, $\dot{y}(0) = 0$, $K = 0.5$, $b = 2$ s, and $\xi = 1$ s. The control is given by RCAC/PID with $G_{\mathrm{f}}(\mathbf{q}) = -1/\mathbf{q}$, RCAC/PID with $G_{\mathrm{f}}(\mathbf{q}) = -(\mathbf{q}-2)/\mathbf{q}^2$, RCAC/PID with $G_{\mathrm{f}}(\mathbf{q}) = -(\mathbf{q}-10)/\mathbf{q}^2$, and DDRCAC/PID.

Example 5.3: Multicopter with unknown dynamics. Let $\mathcal{M}$ be given by the nonlinear multicopter dynamics (4)–(9) and (11)–(16) in [26]. The control objective is to follow a second-order Hilbert curve at a constant altitude in the absence of a disturbance. The control architecture is given by an inner-outer loop configuration in which multiple SISO PID controllers are implemented. The inner-loop control architecture is given by Figure 3 in [17] and the outer-loop control architecture Figure 6 in [17]. The inner-loop architecture implements fixed-gain PID controllers. RCAC/PID and DDRCAC/PID controllers are placed in parallel with fixed-gain PID controllers in the outer-loop architecture to adaptively improve command following performance, similarly to [17]. Two controllers (P for the position loop and PI for the velocity loop) are cascaded for each of the three displacements, that is, along the x, y, and z axes. Hence,

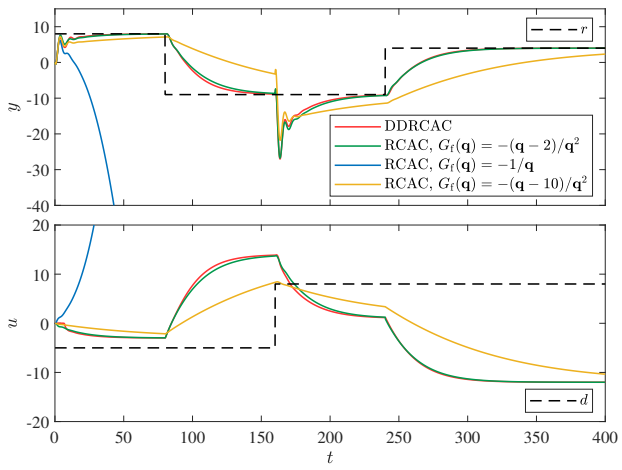

Fig. 6: Example 5.2: Control of the second-order linear NMP plant dynamics (46) with $y(0) = 0$, $\dot{y}(0) = 0$, $K = 0.5$, $b = 2$ s, and $\xi = 0.3$ s. The control is given by RCAC/PID with $G_{\mathrm{f}}(\mathbf{q}) = -1/\mathbf{q}$, RCAC/PID with $G_{\mathrm{f}}(\mathbf{q}) = -(\mathbf{q}-2)/\mathbf{q}^2$, RCAC/PID with $G_{\mathrm{f}}(\mathbf{q}) = -(\mathbf{q}-10)/\mathbf{q}^2$, and DDRCAC/PID.

3 P and 3 PI controllers are required by the outer-loop architecture. The D gain is not used in this application.

Let $G_{\mathrm{f,vxy}}$ be the target model corresponding to the adaptive RCAC PI controllers implemented in the velocity loop for control over the x and y axes. The results of the numerical simulations, where the control is given by RCAC/PID with $G_{\mathrm{f,vxy}}(\mathbf{q}) = -0.5/\mathbf{q}$, RCAC/PID with $G_{\mathrm{f,vxy}}(\mathbf{q}) = 0.5/\mathbf{q}$, and DDRCAC/PID, are shown in Figures 7, 8, and 9. Note that the closed-loop system is unstable when RCAC/PID is implemented with $G_{\mathrm{f,vxy}}(\mathbf{q}) = 0.5/\mathbf{q}$, since an incorrect gain is specified in the target model of a subset of all implemented RCAC/PID controllers. In contrast, DDRCAC/PID does not require this information. ◇

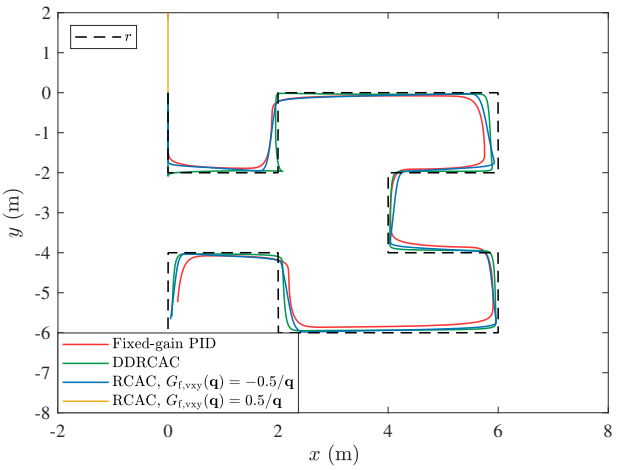

Fig. 7: Example 5.3: Position control of the nonlinear multicopter dynamics (4)–(9) and (11)–(16) in [26]. The plot shows the projection of the trajectory of the multicopter and the commanded trajectory over the $x-y$ plane. The control is given by RCAC/PID with $G_{\mathrm{f,vxy}}(\mathbf{q}) = -0.5/\mathbf{q}$, RCAC/PID with $G_{\mathrm{f,vxy}}(\mathbf{q}) = 0.5/\mathbf{q}$, and DDRCAC/PID.

VI. Conclusions

This paper introduced an adaptive digital PID controller for discrete-time output-feedback control of continuous-time systems. The gains of the PID controller are updated at each step by DDRCAC, which uses VRF-RLS to provide RCAC

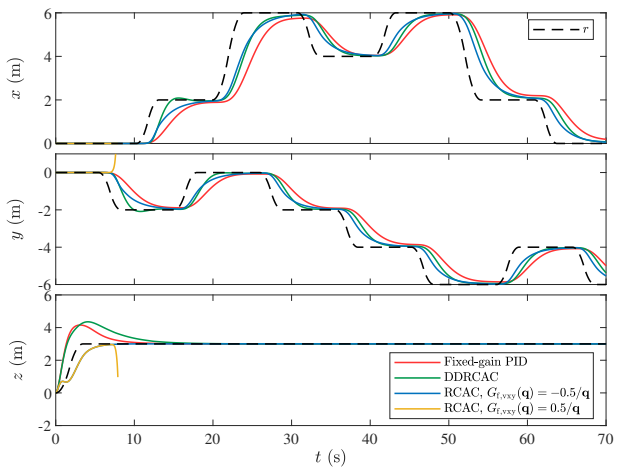

Fig. 8: Example 5.3: Position control of the nonlinear multicopter dynamics (4)–(9) and (11)–(16) in [26]. The plot shows the trajectory of the multicopter along the x, y, and z axes and the commanded trajectory versus time. The control is given by RCAC/PID with $G_{\mathrm{f,vxy}}(\mathbf{q}) = -0.5/\mathbf{q}$, RCAC/PID with $G_{\mathrm{f,vxy}}(\mathbf{q}) = 0.5/\mathbf{q}$, and DDRCAC/PID.

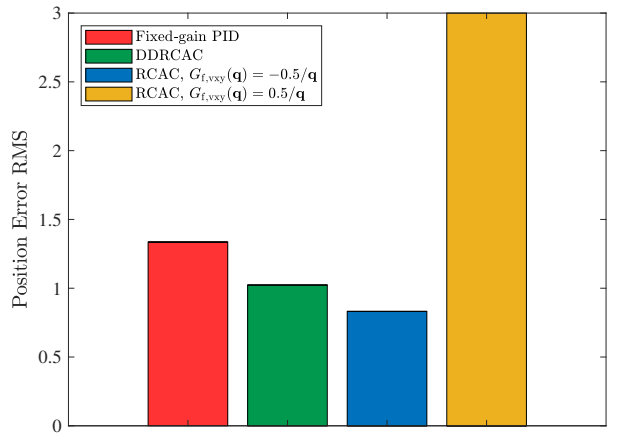

Fig. 9: Example 5.3: Root mean square (RMS) of the 3D position error for the multicopter flights, where the control is given by RCAC/PID with $G_{\mathrm{f,vxy}}(\mathbf{q}) = -0.5/\mathbf{q}$, RCAC/PID with $G_{\mathrm{f,vxy}}(\mathbf{q}) = 0.5/\mathbf{q}$, and DDRCAC/PID.

with the required modeling information in the form of a target model that is updated at each time step. Numerical examples illustrate the performance of this technique and provide a comparison with RCAC-based digital PID control using a fixed target model. Future work will focus on experimental implementation of this approach on a multicopter, where the goal is to improve trajectory tracking with an unknown suspended payload as well as under actuator failure scenarios.

Acknowledgments

This research was supported by ONR under grant N00014-18-1-2211 and AFOSR under grant FA9550-20-1-0028. The authors thank Dr. Ankit Goel for providing the multicopter simulation model used in the numerical simulations.

References

[1] K. Astrom and T. Hagglund, *Advanced PID Control*. ISA, 2006.

[2] A. O'dwyer, *Handbook of PI and PID Controller Tuning Rules*. World Scientific, 2009.

[3] J. Penttinen and H. N. Koivo, "Multivariable tuning regulators for unknown systems," *Automatica*, vol. 16, no. 4, pp. 393–398, 1980.

[4] L. Zaccarian and A. R. Teel, *Modern Anti-Windup Synthesis: Control Augmentation for Actuator Saturation*. Princeton University Press, 2011.

[5] K. J. Åström, T. Hägglund, C. C. Hang, and W. K. Ho, "Automatic tuning and adaptation for PID controllers-a survey," in *Adaptive Systems in Control and Signal Processing*, M. M. L. Dugard and I. Landau, Eds., 1993, pp. 371–376.

[6] H. Logemann and E. P. Ryan, "Time-varying and adaptive integral control of infinite-dimensional regular linear systems with input nonlinearities," *SIAM J. Contr. Optim.*, vol. 38, no. 4, pp. 1120–1144, 2000.

[7] J. W. Jung, V. Q. Leu, T. D. Do, E. K. Kim, and H. H. Choi, "Adaptive PID speed control design for permanent magnet synchronous motor drives," *IEEE Trans. Power Elec.*, vol. 30, no. 2, pp. 900–908, 2015.

[8] J. Berner, K. Soltesz, T. Hägglund, and K. J. Åström, "An experimental comparison of PID autotuners," *Contr. Eng. Practice*, vol. 73, pp. 124–133, 2018.

[9] H. Habibi, H. R. Nohooji, and I. Howard, "Adaptive PID control of wind turbines for power regulation with unknown control direction and actuator faults," *IEEE Access*, vol. 6, pp. 37 464–37 479, 2018.

[10] R. De Keyser, C. I. Muresan, and C. M. Ionescu, "Universal direct tuner for loop control in industry," *IEEE Access*, vol. 7, pp. 81 308–81 320, 2019.

[11] K. J. Åström and B. Wittenmark, "On self-tuning regulators," *Automatica*, vol. 9, no. 2, pp. 185–199, 1973.

[12] R. Isermann, "On advanced methods of process computer control for industrial processes," *IFAC Proc. Vol.*, vol. 11, no. 1, pp. 411–421, 1978.

[13] R. Kurokawa, T. Sato, R. Vilanova, and Y. Konishi, "Closed-loop data-driven trade-off PID control design," *IFAC-PapersOnLine*, vol. 51, no. 4, pp. 244–249, 2018.

[14] S. Formentin, M. C. Campi, A. Carè, and S. M. Savaresi, "Deterministic continuous-time virtual reference feedback tuning (VRFT) with application to PID design," *Sys. Contr. Lett.*, vol. 127, pp. 25–34, 2019.

[15] Y. Rahman, A. Xie, and D. S. Bernstein, "Retrospective Cost Adaptive Control: Pole Placement, Frequency Response, and Connections with LQG Control," *IEEE Contr. Sys. Mag.*, vol. 37, pp. 28–69, Oct. 2017.

[16] M. Kamaldar, S. A. U. Islam, S. Sanjeevini, A. Goel, J. B. Hoagg, and D. S. Bernstein, "Adaptive digital PID control of first-order-lag-plus-dead-time dynamics with sensor, actuator, and feedback nonlinearities," *Adv. Contr. Appl.*, vol. 1, no. 1, p. e20, 2019.

[17] A. Goel, J. A. Paredes, H. Dadhaniya, S. A. Ul Islam, A. M. Salim, S. Ravela, and D. Bernstein, "Experimental Implementation of an Adaptive Digital Autopilot," in *Proc. Amer. Contr. Conf.* IEEE, 2021, pp. 3737–3742.

[18] J. Spencer, J. Lee, J. A. Paredes, A. Goel, and D. Bernstein, "An adaptive PID autotuner for multicopters with experimental results," in *Proc. Int. Conf. Robot. Automat.* IEEE, 2022, pp. 7846–7853.

[19] J. Lee, J. Spencer, S. Shao, J. A. Paredes, D. S. Bernstein, and A. Goel, "Experimental flight testing of a fault-tolerant adaptive autopilot for fixed-wing aircraft," in *Proc. Amer. Contr. Conf.* IEEE, 2023, pp. 2981–2986.

[20] S. A. U. Islam, T. Nguyen, I. Kolmanovsky, and D. S. Bernstein, "Data-Driven Retrospective Cost Adaptive Control for Flight Control Applications," *J. Guid. Contr. Dyn.*, vol. 44, pp. 1732–1758, October 2021.

[21] S. A. U. Islam and D. S. Bernstein, "Recursive least squares for real-time implementation," *IEEE Contr. Syst. Mag.*, vol. 39, no. 3, pp. 82–85, 2019.

[22] A. L. Bruce, A. Goel, and D. S. Bernstein, " Convergence and Consistency of Recursive Least Squares with Variable-Rate Forgetting," *Automatica*, vol. 119, p. 109052, 2020.

[23] N. Mohseni and D. S. Bernstein, "Recursive least squares with variable-rate forgetting based on the F-test," in *Proc. Amer. Contr. Conf.*, 2022, pp. 3937–3942.

[24] K. J. Åström and B. Wittenmark, *Computer-Controlled Systems: Theory and Design, Third Edition*. Dover Publications, 2013.

[25] E. D. Sumer and D. S. Bernstein, "Retrospective cost adaptive control with error-dependent regularization for MIMO systems with uncertain nonminimum-phase transmission zeros," in *Proc. AIAA Guid. Nav. Contr. Conf.*, 2012, AIAA-2012-4670-123.

[26] A. Goel, A. M. Salim, A. Ansari, S. Ravela, and D. Bernstein, "Adaptive digital PID control of a quadcopter with unknown dynamics," *arXiv preprint arXiv:2006.00416*, 2020.